



# Experimental characterization of a novel soft polymer heat exchanger for wastewater heat recovery

Sixiang Lyu<sup>a</sup>, Cheng Wang<sup>b,\*</sup>, Chuanyu Zhang<sup>c</sup>, Laurent Royon<sup>c</sup>, Xiaofeng Guo<sup>c,d,\*\*</sup>

<sup>a</sup> Department of Energy Technology, KTH Royal Institute of Technology, Stockholm, Sweden

<sup>b</sup> Jiangsu Provincial Key Laboratory of Oil & Gas Storage and Transportation Technology, Changzhou University, Changzhou, Jiangsu, PR China

<sup>c</sup> Université de Paris, CNRS, LIED, UMR 8236, F-75006 Paris, France

<sup>d</sup> Université Gustave Eiffel, ESIEE Paris, F-93162 Noisy le Grand, France

## ARTICLE INFO

### Article history:

Received 10 May 2020

Revised 16 July 2020

Accepted 23 July 2020

### Keywords:

Polymer heat exchanger

Wastewater

Heat recovery

Heat transfer enhancement

Oscillation

Serpentine-like

## ABSTRACT

Wastewater released from showers, sinks, and washers contains a considerable amount of waste heat that can be recovered by using a heat exchanger. Conventional metal heat exchangers for wastewater heat recovery have common problems of corrosion, fouling and clogging, which makes it necessary to develop a new type of heat exchanger for such low-grade thermal energy recovery applications. This study deals with a novel patented polymer heat exchanger (WO2020049233A1) made of soft polyurethane tubes that are capable of oscillation once subjected to external forces. Laboratory tests coupled with theoretical analyses show a stable global heat transfer coefficient of 100–110 W/m<sup>2</sup>·K, achieving 67–92% of the performance of titanium-, aluminum-, and copper-made heat exchangers with the same configuration. It further reveals that the performance of the soft heat exchanger can be enhanced by 30% when it is under oscillation. In addition, the external convective thermal resistance appears to be the dominant one instead of heat conduction through the wall material. The special operating condition of heat recovery from a sewer pipeline makes the polymer heat exchanger particularly adapted with its equivalent thermal performance but advantages of high flexibility, modularity, and low cost.

© 2020 Elsevier Ltd. All rights reserved.

## 1. Introduction

The growing world urbanization and climate change bring imminent challenges for the sustainable development of the society. A recent study by U.S. Energy Information Administration [1] predicted an increase in world energy consumption by nearly 50% between 2018–2050, of which almost all the increase comes from non-OECD countries having strong economic growth and rapid urbanization pace. Cities appear to dominate energy consumption and CO<sub>2</sub> emissions. In 2013, the world's urban areas accounted for about 64% of global primary energy use and produced 70% of the total CO<sub>2</sub> emissions [2]. More recently, the Covid-19 crisis inevitably urge the society to strengthen efforts made to the energy-climate transition.

Accessible, low-cost and stable alternative solutions are key to replace fossil-based energy. One way is to expand the share of re-

newable energies, such as solar photovoltaic (PV), wind, and bioenergy. However, this usually requires a considerable amount of financial support and their implementation is severely dependent on policy implementation, including the building of new energy infrastructures. Moreover, PV might be in conflict with agriculture when it comes to land occupation, while bioenergy can be in competition with food. The mismatch between demand and renewable production can also be problematic [3]. An alternative solution is to increase energy efficiency by reusing or converting waste energy (mostly in the form of heat) to other forms of energy from existing systems.

In recent years, wastewater in urban sewer networks has attracted extensive interest for thermal energy recovery because of its easy accessibility and high abundance. Wastewater released from showers, sinks, and drains contains significant quantities of thermal energy, much higher than organic energy [4]. An amount of 1.16 kWh thermal energy can be gained, if 1 m<sup>3</sup> of water is cooled down by 1°C. According to Mazhar et al. [5], approximately 3.5 kWh of thermal energy per person per day could be harvested and used directly to meet thermal demands. Moreover, reusing heat from wastewater also helps to reduce greenhouse gas emissions. Takashi et al. [6] conducted a feasibility study in wastewater

\* Corresponding author.

\*\* Corresponding author at: Université Gustave Eiffel, ESIEE Paris, department SEN, F-93162 Noisy le Grand, France.

E-mail addresses: [wangcheng3756@163.com](mailto:wangcheng3756@163.com) (C. Wang), [xiaofeng.guo@esiee.fr](mailto:xiaofeng.guo@esiee.fr) (X. Guo).

## Nomenclature

$A$	Heat transfer area of the pipe [m <sup>2</sup> ]
$A_c$	Cross-sectional area of the pipe [m <sup>2</sup> ]
$c_p$	Specific heat capacity of water [J/kg·K]
$D$	Diameter of the pipe [m]
$f$	Friction factor [-]
$h$	Convective heat transfer coefficient [W/m <sup>2</sup> ·K]
$k$	Thermal conductivity of the fluid [W/m·K]
$L$	Length of a unit pipe [m]
$LMTD$	Logarithmic mean temperature difference [K]
$\dot{m}$	Mass flow rate [kg/s]
$N$	Number of peripheric pipes [-]
$Nu$	Nusselt number [-]
$P$	Wetted perimeter of the pipe [m]
$Pr$	Prandtl number [-]
$\dot{Q}$	Heat transfer rate [W]
$R$	Thermal resistance [K/W]
$Re$	Reynolds number [-]
$T$	Temperature [°C]
$u$	Fluid velocity [m/s]
$U$	Overall heat transfer coefficient [W/m <sup>2</sup> ·K]
$UA$	Heat conductance [W/K]
<i>Greek symbols</i>	
$\lambda$	Thermal conductivity of polymer material [W/m·K]
$\mu$	Fluid dynamic viscosity [Pa·s]
$\rho$	Fluid density [m <sup>3</sup> /kg]
<i>Subscripts</i>	
Al	Aluminum
c	Central pipe
Cu	Copper
$D$	Diameter
h	Hydraulic
HTF	Heat transfer fluid
i	Pipe inside
in	Inlet
m	Middle
o	Pipe outside
out	Outlet
p	Peripheric pipe
s	Surface
tot	Total
Ti	Titanium
w	Water in LMTD calculation / Wall in thermal resistance

heat recovery and concluded that 2.5 tons of CO<sub>2</sub> can be avoided per 10 000 m<sup>3</sup> of wastewater. Guo and Hendel [7] performed a case study in Paris to evaluate the field performance of a district-scale wastewater heat recovery system with an effluent flow rate of 115 m<sup>3</sup>/h, and reported that up to 75% CO<sub>2</sub> could be reduced annually with a primary energy savings of 32%. Cold recovery case studies have also been carried out in Amsterdam drinking water network by van der Hoek et al. [8].

Conventionally, there are two techniques to extract heat from wastewater in urban sewer channels by means of heat exchangers. There are already some existing systems or demonstrating projects using both technologies worldwide [9–12]. The first technique (integrated system) is to install a metal-made tubular heat exchanger at the bottom of the sewer pipeline [7,13]. Several tubular exchangers with long length are often connected in series to achieve the desired heat capacity, due to their relative small heat exchanger surface and low heat transfer coefficient [7]. Apart from weight

and cost, metal heat exchangers also have issues of corrosion and fouling that often cause low efficiency or even failures [14,15]. Moreover, in sewer pipes, the efficiency of the heat exchanger will be largely reduced if its surface is surrounded by sediments or biofilms or is not completely submerged [13].

The second technique (external system) is to pump the wastewater to a heat exchanger installed outside of the sewer. Spiral heat exchangers with advantages of compact design, large exchange surface, and high heat transfer coefficient are usually used in this technique [16]. Besides, the high-speed flow through spiral heat exchangers can reduce the effect of fouling. However, it requires a dedicated by-pass piping network and high installation and pumping costs [13]. Also, regular maintenance is necessary to avoid clogging by solid matters in wastewater.

Hence, facing this new application, it is desirable to find a solution to overcome those problems associated with metal heat exchangers. One promising solution is to use polymer materials instead of metals for manufacturing heat exchangers. Many different polymer materials have been studied for their physicochemical properties, such as polypropylene (PP), polyethylene (PE), polycarbonate (PC), polytetrafluoroethylene (PTFE), etc. [15,17]. These materials have advantages of greater corrosion and fouling resistance, higher geometric flexibility, and they are easier to manufacture with reduced energy of formation and fabrication [15,17]. The use of polymer heat exchangers also helps to reduce transportation and installation costs, which eventually lowers the total investment [14].

Nevertheless, polymer materials have significant low thermal conductivities of typically less than 0.5 W/m·K compared to most metals which range from 10 W/m·K to 400 W/m·K [15]. Therefore, extensive research has been carried out to improve the thermal performance of polymer heat exchangers. The commonly used technique is to dope the polymer thermal conductivity by adding metal, ceramic, or carbon-based particles into the polymer matrix [15]. Breuer and Sundararaj [18] reported that the thermal conductivity of PP could be increased by 120% with 1 wt.% loading of single-walled carbon nanotubes (SWCNTs). Mamuya et al. [19] studied the thermal conductivity of polyvinyl chloride (PVC) filled with copper powders at different filler volume contents and reported 3–4 times thermal conductivity improvements with a filler volume content of 30%. Compared with the thermal performance of metal heat exchangers, Chen et al. [14] have shown that a modified PP heat exchanger with thermal conductivity of 15 W/m·K can achieve 95% of the titanium heat exchanger performance and 84% of the aluminum or copper heat exchanger performance with the same dimensions.

In addition to conductivity enhancement of polymers, the operating condition, in particular vibration or other movements, also have potentially high impacts on heat exchanger performance. Recently, vibration effects on heat transfer enhancement have been confirmed numerically or experimentally. Shi et al. [20] numerically studied heat transfer enhancement by Vortex-Induced Vibration (VIV) generated by a cylindrical obstacle in a channel. Their results indicate that VIV can significantly increase the average Nusselt number up to 90.1% over that of a smooth channel. Liu et al. [21] used an experimental approach to study the effects of mechanical vibration on heat transfer characteristics of laminar flow in a circular heated tube. An increased Nusselt number and a maximum heat transfer enhancement of 14.94% was found owing to the vibration. A more sophisticated technique is to use ultrasonic vibration to enhance heat transfer. Chen et al. [22] investigated the heat transfer enhancement under ultrasonic vibration using a stainless steel circular heater rod, and found a maximum heat transfer increment of 1 557 W/m<sup>2</sup>·K with an increment ratio of 3.01. In terms of energy input, however, their ultrasonic transducer requires a total power of 150 W with a frequency of 40 Hz.

Undesirable local heating could be problematic for the use of ultrasounds [23,24]. To our knowledge, the use of unmodified polymer heat exchanger in sewer wastewater heat recovery has yet not appeared in the literature.

In this paper, we report a newly patented polymer heat exchanger (WO2020049233A1) designed for wastewater heat recovery from sewers [25]. Laboratory experiments are carried out to determine its heat transfer characteristics, including heat transfer rate, heat transfer coefficient, and thermal resistance. As a unique advantage, oscillational movement of the soft heat exchanger is also studied to explore the heat transfer enhancement potential compared with standstill position (which is true to all classical rigid heat exchangers). In the absence of established correlation for serpentine-shape cylinder heat convection, theoretical results obtained from ideal models of parallel flow and crossflow heat exchanger with the same dimension and working conditions are used to define the upper and lower performance limits of the studied heat exchanger. Based on the model, the sensibility of heat exchanger performance on material thermal conductivity allows the comparison with metal heat exchangers. The data and results from this paper may offer some reference for the design and use of polymer heat exchanger in wastewater heat recovery or similar applications.

## 2. Polymer heat exchanger

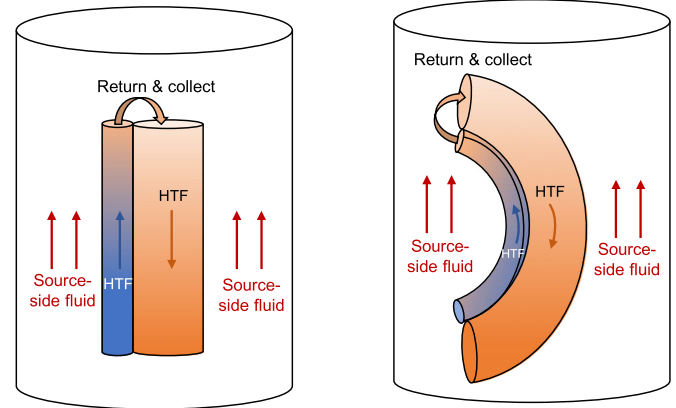
### 2.1. Design and dimensions

Fig. 1 shows schematically the structure of the novel heat exchanger and the dimension of the tested prototype. The heat exchanger is made of polymer polyurethane (PU), consisting of ten peripheric pipes and one central pipe [25]. The pipes are connected at one end by a cap for fluid return and this end is freely immersed in the source-side fluid (wastewater). The peripheric pipes (Port 1) and central pipe (Port 2) at the other end allow the feeding and return of the heat transfer fluid (HTF).

Manufactured by extrusion, this soft polymer heat exchanger holds important advantages of high modularity and flexibility. Namely, it can be prefabricated then cut into any length according to the capacity requirement or installation environment. The heat exchanger can be operated at four different modes depending on the direction of HTF flow and relative temperatures between the HTF and source-side fluid, as shown in Table 1. Heat recovery refers to the situations when HTF temperature is lower than that of the source-side, while cold recovery refers to

**Table 1**  
Different operating modes of the polymer heat exchanger.

Cases	Port 1	Port 2	Relative temperature	Type of recovery
Case 1	HTF in	HTF out	$T_{HTF} < T_{source}$	Heat recovery
Case 2	HTF out	HTF in	$T_{HTF} < T_{source}$	Heat recovery
Case 3	HTF in	HTF out	$T_{HTF} > T_{source}$	Cold recovery
Case 4	HTF out	HTF in	$T_{HTF} > T_{source}$	Cold recovery



**Fig. 2.** Schematic view of the heat exchanger in different positions and their corresponding fluid flow patterns (left: straight position with parallel flow; right: serpentine position with mixed parallel-cross flow).

the cases when HTF temperature is higher than the source-side fluid.

### 2.2. Flow patterns

The soft nature of the material, together with the one end in free movement, makes the heat exchanger be easily deformed during operation due to external forces (turbulent flow, natural convection, thermocline, vortices, etc.). The deformation of the heat exchanger changes not only the shape but also the flow pattern between the HTF and source-side fluid. Fig. 2 illustrates positions of the heat exchanger (only one peripheric pipe is shown instead of ten) in both straight and serpentine positions and their corresponding flow patterns. In the straight position, parallel flow dominates heat transfer between the HTF and source-side fluid, with peripheric pipes being co-current and the central pipe in counter-current configuration. However, a crossflow is created when the

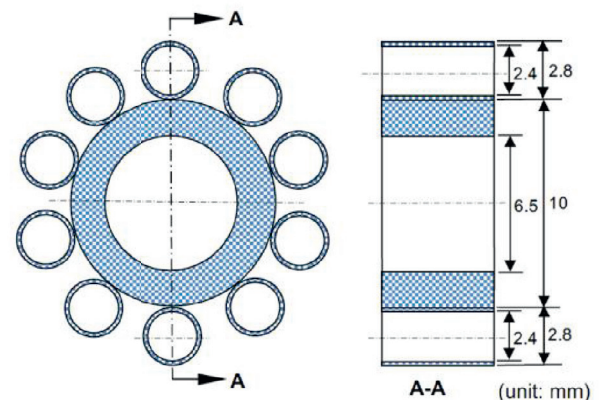
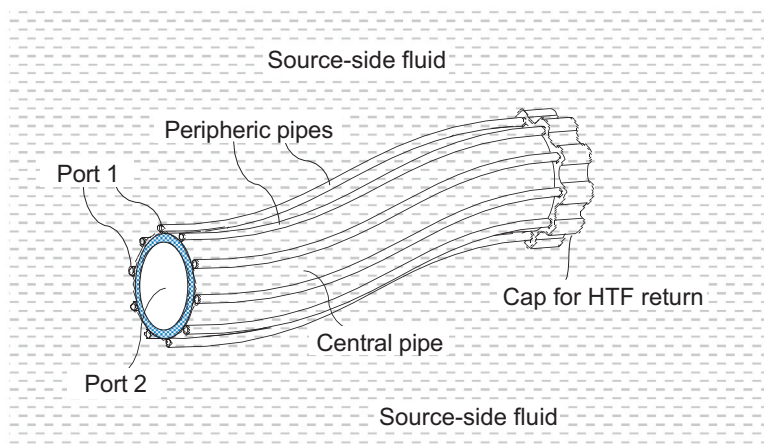


**Fig. 1.** Basic structure of the soft polymer heat exchanger (left) and dimension of the pipes (right).

heat exchanger is in the serpentine position, which could enhance the external convection. Moreover, previous studies [26,27] have shown that Dean vortices can be formed when a fluid flows in a curved channel, resulting in an enhanced internal convective heat transfer. In sum, the facility of deformation of the novel heat exchanger makes it potentially more performant compared to a rigid heat exchanger under equal material and operating conditions.

### 3. Theoretical model

#### 3.1. Overall heat transfer coefficient

The overall heat exchange coefficient ( $U$ ) depends on those of peripheric ( $U_p$ ) and central pipes ( $U_c$ ). Each of them depends on internal and external convection and conduction through walls. The thermal resistances for internal convective ( $R_i$ ), external convective ( $R_o$ ), and conductive heat transfer through walls ( $R_w$ ) can be calculated using the Eqs. (1)-(3) [27], hence the total thermal resistance is the sum of them by Eq. (4):

$$R_i = \frac{1}{\pi h_i D_i N L} \quad (1)$$

$$R_o = \frac{1}{\pi h_o D_o N L} \quad (2)$$

$$R_w = \frac{\ln\left(\frac{D_o}{D_i}\right)}{2\pi \lambda N L} \quad (3)$$

$$R_{tot} = R_i + R_o + R_w \quad (4)$$

The overall heat transfer coefficient of the peripheric pipes or central pipe may be determined as follows [27]:

$$U_p = \frac{1}{A_p \cdot R_{tot,p}} \quad (5)$$

$$U_c = \frac{1}{A_c \cdot R_{tot,c}} \quad (6)$$

The global heat transfer coefficient of the entire heat exchanger is finally calculated by the sum of the overall heat transfer coefficient of each pipe to the ratio of heat transfer area as shown in Eq. (7):

$$U = U_p \cdot \frac{A_p}{A_p + A_c} + U_c \cdot \frac{A_c}{A_p + A_c} \quad (7)$$

Substituting Eqs. (5) and (6) in (7), the Eq. (7) becomes:

$$U = \frac{1}{A \cdot R_{tot,p}} + \frac{1}{A \cdot R_{tot,c}} \quad (8)$$

#### 3.2. Internal convective heat transfer coefficient

To determine the internal convective heat transfer coefficient ( $h_i$ ), the Reynolds number of internal tube flow is calculated to determine the flow regime:

$$Re_D = \frac{u \rho D_i}{\mu} \quad (9)$$

For internal pipe flow, the flow can be considered as laminar flow if  $Re_D < 2300$ , and turbulent if  $Re_D > 2900$  [27]. It worth noting that for  $N$  peripheric pipes, the mean velocity  $u$  is calculated by the  $\dot{m}_p$  being divided by  $N$  ( $N=10$ ).

In the case of fully developed laminar flow with constant surface temperature, and without considering the entrance development zone, the Nusselt number can be considered as constant:

$$Nu_D = 3.66 \text{ if } T_s = \text{constant} \quad (10)$$

For turbulent flow, the correlation provided by Gnielinski [27] is used to determine the Nusselt number:

$$Nu_D = \frac{(f/8)(Re_D - 1000)Pr}{1 + 12.7(f/8)^{1/2}(Pr^{2/3} - 1)} \quad (11)$$

This correlation is valid for  $0.5 \leq Pr \leq 2000$  and  $3000 \leq Re_D \leq 5 \cdot 10^6$ , and it can be applied for both constant heat flux and temperature conditions. In the equation, the Darcy friction factor  $f$  can be obtained from the Churchill equation (1977) [28] that is valid for all flow regimes:

$$f = 8 \cdot \left[ \left( \frac{8}{Re} \right)^{12} + \left( \left\{ 2.457 \cdot \ln \left( \frac{1}{\left( \frac{7}{Re} \right)^{0.9} + 0.27 \frac{\varepsilon}{D_i}} \right)} \right\}^{16} + \left( \frac{37530}{Re} \right)^{16} \right)^{-1.5} \right]^{\frac{1}{12}} \quad (12)$$

where  $\varepsilon$  and  $D_i$  are the surface roughness (0.0015 mm for PU) and the inner diameter of the pipe.

Once  $Nu_D$  is obtained, the internal convective heat transfer coefficient of the peripheric or central pipe is determined by Eq. (13):

$$h_i = \frac{Nu_D k}{D_i} \quad (13)$$

#### 3.3. External heat transfer coefficient

The external convection coefficient ( $h_o$ ) depends on the relative flow pattern between the HTF and source-side fluid. As the soft heat exchanger is in a serpentine position, the complex flow pattern involves both parallel and crossflow, the latter being more favorable to convective heat transfer. Thus, the external convection coefficient around a serpentine-cylinder should be limited by values obtained by parallel and crossflow correlations.

In parallel flow, the external convective heat transfer coefficient is calculated by considering the peripheric and central pipe to be a single united pipe. This united pipe together with the external water pipeline acts as a concentric tube annulus. The hydraulic diameter of the concentric tube annulus is calculated using Eq. (14):

$$D_h = \frac{4A_c}{P} = \frac{D_{ti}^2 - 10D_{po}^2 - D_{co}^2}{D_{ti} + 10D_{po} + D_{co}} \quad (14)$$

Then, Eq. (9) allows determining Reynolds number with  $D_h$  in place of  $D_i$ . The flow regime is laminar with calculated  $Re = 745$  (source-side fluid flow rate 60 g/s) and for the case of fully developed laminar flow in an annulus, with one surface insulated and another surface at a constant temperature,  $Nu_o$  entirely depends on the geometry of the concentric tube. Rohsenow et al. suggest  $Nu_o = 4.17$  [29].

The external convective heat transfer coefficient is then determined using:

$$h_o = \frac{Nu_o k}{D_h} \quad (15)$$

In the case of crossflow, the flow structure can no longer be considered as an annulus, Eq. (14) for calculating hydraulic diameter is adjusted to Eq. (16) as follows [27]:

$$D_h = \frac{D_{co}^2 + 10D_{po}^2}{D_{co} + 10D_{po}} \quad (16)$$

To determine the Nusselt number on the external surface with calculated  $Re$  of about 52, the correlation for  $Re < 500$  presented by Hsu (1963) is used [30], as shown in Eq. (17). Although Churchill and Bernstein (1977) correlation [27] covers a larger range of  $Re$

through a single equation, the current study uses fixed source-side flow rate having constant Re, which makes Eq. (17) sufficient.

$$Nu = 0.43 + 0.48Re^{\frac{1}{2}} \quad (17)$$

The formula for the external convective heat transfer coefficient in crossflow remains the same as described in Eq. (15).

### 3.4. Heat transfer rates

The heat transfer rate of the heat exchanger is calculated with the outlet temperatures determined by using the Logarithmic Mean Temperature Difference (LMTD) method. For the peripheric pipe and central pipe, the LMTD is expressed in Eqs. (18) and (19) [27]:

$$LMTD_p = \frac{(T_{w,out} - T_{HTF,m}) - (T_{w,in} - T_{HTF,in})}{\ln\left(\frac{T_{w,out} - T_{HTF,m}}{T_{w,in} - T_{HTF,in}}\right)} \quad (18)$$

$$LMTD_c = \frac{(T_{w,out} - T_{HTF,m}) - (T_{w,in} - T_{HTF,out})}{\ln\left(\frac{T_{w,out} - T_{HTF,m}}{T_{w,in} - T_{HTF,out}}\right)} \quad (19)$$

It is worth noting the expression of LMTD is based on co-current flow pattern for peripheric pipes and counter-current flow for the central one. This is furtherly illustrated in Fig. 4.

Similarly, the heat conductance (UA) can be obtained for the peripheric and central pipe from Eqs. (5) and (6) as follows:

$$(UA)_p = \frac{1}{R_{tot,p}} \quad (20)$$

$$(UA)_c = \frac{1}{R_{tot,c}} \quad (21)$$

The outlet temperatures, including the middle and outlet temperature of the HTF fluid ( $T_{HTF,m}$ ,  $T_{HTF,out}$ ) and the outlet temperature of the source-side fluid ( $T_{w,out}$ ), can be derived by solving a system of three equations (22)-(24) with known information of inlet temperatures, flow rates, and heat conductance.

$$(UA)_p LMTD_p = \dot{m}_{HTF} c_{p,HTF} (T_{HTF,m} - T_{HTF,in}) \quad (22)$$

$$(UA)_c LMTD_c = \dot{m}_{HTF} c_{p,HTF} (T_{HTF,out} - T_{HTF,m}) \quad (23)$$

$$\dot{m}_w c_{p,w} (T_{w,out} - T_{w,in}) = \dot{m}_{HTF} c_{p,HTF} (T_{HTF,in} - T_{HTF,out}) \quad (24)$$

With the solved outlet temperatures, the heat transfer rate is obtained respectively for the peripheric pipe and central pipe using the heat transfer equations (25)-(26). The global heat transfer rate is the sum of two components in series (Eq. (27)).

$$\dot{Q}_p = \dot{m}_p c_{p,HTF} (T_{HTF,in} - T_{HTF,m}) \quad (25)$$

$$\dot{Q}_c = \dot{m}_c c_{p,HTF} (T_{HTF,m} - T_{HTF,out}) \quad (26)$$

$$\dot{Q} = \dot{Q}_p + \dot{Q}_c \quad (27)$$

## 4. Experimental procedure and data analysis

### 4.1. Experimental procedure

The polymer heat exchanger is tested in a temperature-regulated water pipeline (with an internal diameter of 90 mm) for source-side fluid under operating mode Case 1 (Table 1), as shown in Fig. 3. The heat exchanger is designed to have a length of 1.65 m, slightly shorter than the water pipeline. Both HTF and source-side fluid use water, and the inlet temperature of the source-side

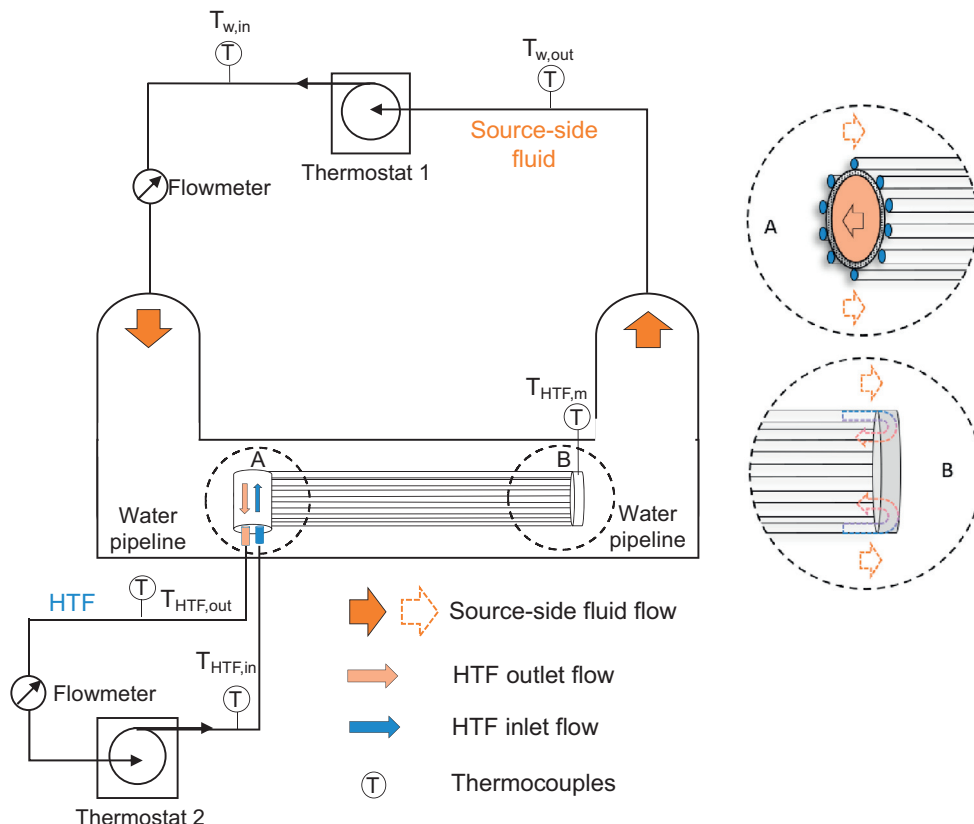


Fig. 3. Schematic of the experimental setup.

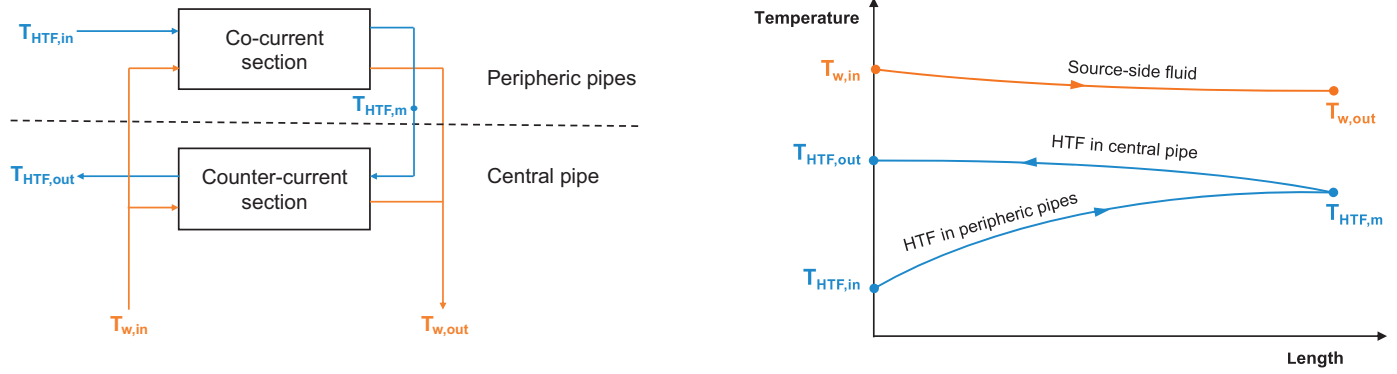


Fig. 4. The heat exchanger model (left) and the expected temperature profile (right) in heat recovery operating mode.

and HTF is maintained at 30°C and 20°C respectively by two thermostats. HTF is fed into the heat exchanger from the peripheric pipes and returned to the thermostat from the central pipe. At the heat exchanger inlet, outlet, and middle point, as well as the inlet and outlet of the water pipeline, fluid temperatures are measured by K-type thermocouples. The HTF-side pressure loss is measured by an AST5100 wet-wet differential pressure transmitter, with corresponding flow rates measured by Coriolis mass flowmeters (mini CORI-FLOW, Bronkhorst). The heat exchanger model and its corresponding temperature profile in this working mode (Case 1) are illustrated in Fig. 4.

During the experimental runs, the flow rate of the source-side fluid is kept at a constant value of 60 g/s. It is 4 to 15 times higher than the HTF flow rate (4.27–15.7 g/s) and allows a reasonable hypothesis of fixed temperature wall condition during heat convection coefficient estimation. The experiment is kept running continuously with varying HTF flow rates to determine its effects on the thermal performance of the heat exchanger. At each level of the HTF flow rates, four representative data points are chosen for further calculation and analysis. As a preliminary study, the influence of oscillation on heat exchanger performance is also tested. The oscillation is created manually by shaking the heat exchanger around its longitudinal axis. With the other end of the soft heat exchanger in free movement, a transient serpentine form is created with an amplitude of  $\pm 35$  mm and under a frequency of 1–2 Hz. Approximately 2–3 sinusoidal cycles constitute the total length of the heat exchanger (1.65 m).

The reading of thermocouples and flowmeters are automatically recorded by a computer. The main measurement uncertainties are from the thermocouples and flowmeters and are within  $\pm 0.5^\circ\text{C}$  and  $\pm 0.1$  g/s, respectively.

#### 4.2. Experimental data analysis

The experimental heat transfer rate between the HTF and source-side fluid can be calculated respectively for the peripheric pipes and central pipe using Eqs. (25) and (26), and the global heat transfer rate is the sum of the two components in series by Eq. (27). The experimental LMTD is estimated using the same Eqs. (18) and (19) for the peripheric pipe and central pipe, respectively.

The heat conductance (UA) is determined as follows using the previously calculated LMTD:

$$(UA)_p = \frac{\dot{Q}_p}{LMTD_p} \quad (28)$$

$$(UA)_c = \frac{\dot{Q}_c}{LMTD_c} \quad (29)$$

The overall heat transfer coefficient (U) can be calculated individually for peripheric and central pipe:

$$U_p = \frac{(UA)_p}{A_p} \quad (30)$$

$$U_c = \frac{(UA)_c}{A_c} \quad (31)$$

Finally, the global heat transfer coefficient of the entire heat exchanger is obtained using the Eq. (7).

## 5. Results and discussion

### 5.1. Temperature profiles

The outlet temperatures ( $T_{w, out}$ ,  $T_{HTF, out}$  and  $T_{HTF, m}$ ) of the polymer heat exchanger obtained from the experiment (EXP), parallel flow (PF), and crossflow (CF) theoretical models by the LMTD method are compared at various HTF flow rates, as shown in Fig. 5. Constant inlet temperatures  $T_{w, in}$  and  $T_{HTF, in}$  are averaged at measured values of 30.14°C and 20.75°C, respectively. As already illustrated in Fig. 4, the HTF temperature lift can be divided into two parts: the temperature lifted in the peripheric pipes ( $T_{HTF, m} - T_{HTF, in}$ ) and the temperature lifted in the central pipe ( $T_{HTF, out} - T_{HTF, m}$ ). Results reveal that, with about three-fold heat

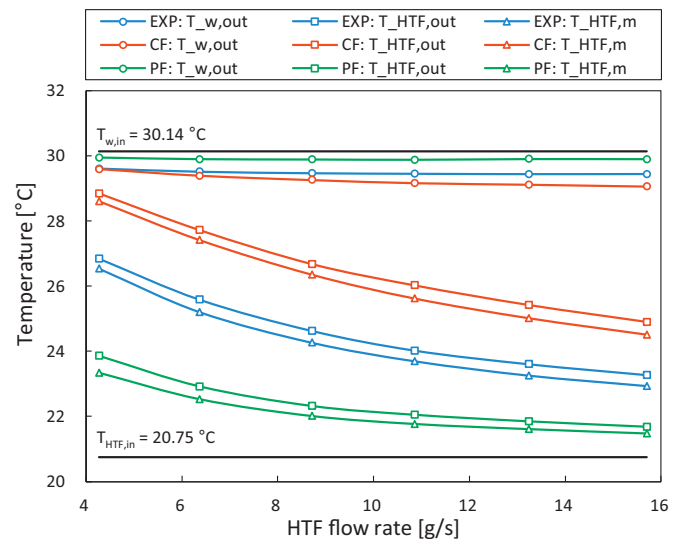
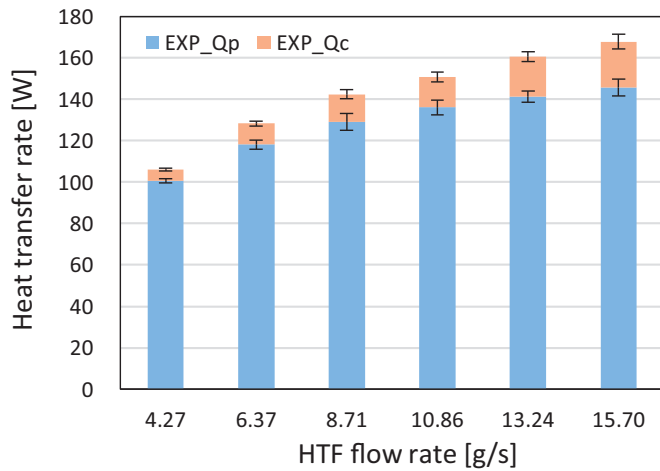


Fig. 5. Comparison of outlet temperatures derived from experiment and theoretical models.



**Fig. 6.** Experimental heat transfer rates for peripheric and central pipes at different HTF flow rates. (Error bars represent the standard deviation for a set of 4 repetitive test results)

transfer area, the temperature lift in the peripheric pipes is substantially higher compared to the central pipe regardless of flow patterns. For example, for the HTF flow rate at 8.71 g/s, the experimental results show HTF temperature is increased from 20.75°C to 24.26°C after the peripheric pipes and then to 24.62°C at the outlet of the central pipe. Moreover, since the flow rate of the source-side fluid (60 g/s) is about 4 to 15 times higher than the HTF flow rate, the temperature change in the source-side fluid is significantly smaller than that of HTF. According to experimental results, the maximum temperature difference in the source-side fluid is as low as 0.7°C while the value is 6.09°C in HTF. In addition, compared with inlet temperatures, the experimental outlet temperatures in both HTF and source-side fluid (water) are between those estimated by parallel flow and crossflow models, with crossflow giving the highest temperature differences. This confirms the particular parallel-cross mixed flow pattern between the serpentine-shape soft heat exchanger and source-side fluid.

### 5.2. Experimental heat transfer rate

Heat transfer rate has been commonly used to evaluate the heat transfer performance of heat exchangers. With Eqs. (25) and (26), the experimental heat transfer rate of the polymer heat exchanger is calculated, and the results are shown in Fig. 6. For both peripheric and central pipes, the heat transfer rate increases with higher HTF flow rates. For the highest flow rate of 15.70 g/s, the total heat transfer rate under the test condition (hot and cold inlets being respectively 30.14°C and 20.75°C) can achieve 168 W, leading to a linear value of 102 W/lm (watt per linear meter). Moreover, the peripheric pipes dominate the performance of the heat exchanger, accounting for 87%–95% of the global heat transfer rate in the tested flow range (22 W for the central pipe and 146 W for peripheric ones in the case of 168 W). This is mainly due to the relatively larger heat transfer surface of the peripheric pipe (0.145 m<sup>2</sup>) than that of the central one (0.052 m<sup>2</sup>).

It worth noting the pressure loss of the HTF side is also measured for all flow rates and results show a maximal pressure drop of 24 588 Pa for the total length of 1.65 m. Details are given in Appendix A1.

### 5.3. Comparison with theoretical models

The characteristics of heat exchanger in crossflow and parallel flow are studied with the theoretical LMTD model, which is validated by NTU- $\epsilon$  method (details in Appendix A2). The results are

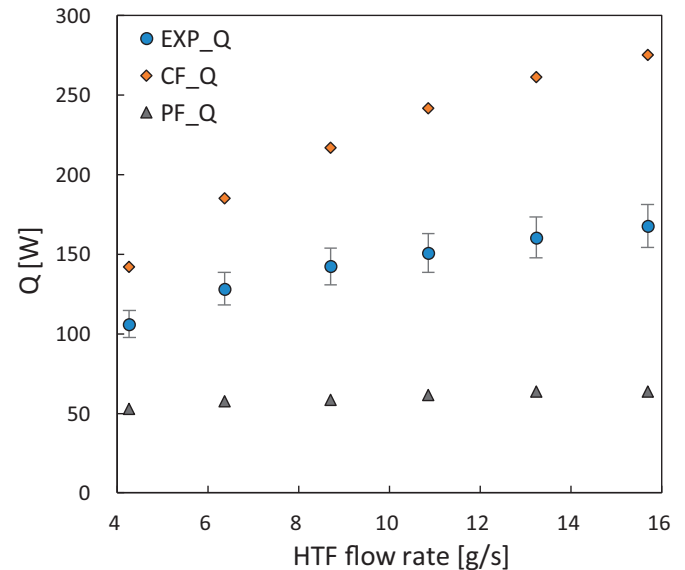


**Fig. 7.** Comparison between experimental and theoretical global heat transfer rate. Experiments are conducted with serpentine-shape heat exchanger in a straight water pipeline, which is a combination of crossflow and parallel flow. The theoretical results from crossflow and parallel flow convection correlation provide upper and lower limits of the heat exchanger performance.

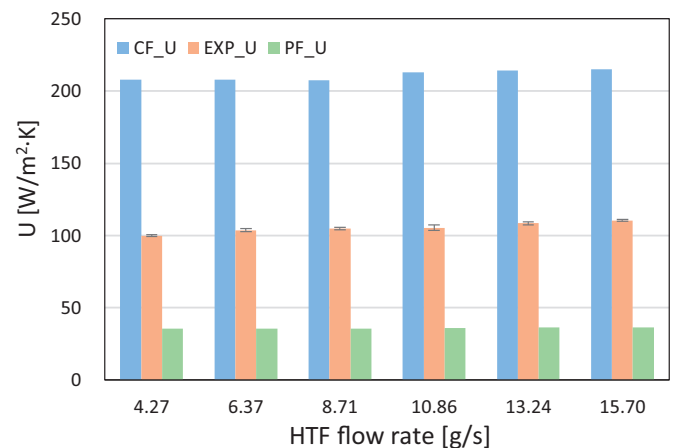


**Fig. 8.** Experimental global heat transfer coefficient and its upper and lower limits provided by theoretical cross-flow (CF) and parallel-flow (PF) models.

**Table 2**

Performance comparison between heat exchanger made of different materials in crossflow.

Heat exchanger material	$\lambda$ [W/m·K]	$U$ [W/m <sup>2</sup> ·K]	$U/U_{Ti}$	$U/U_{Al}$	$U/U_{Cu}$
Polyurethane (PU)	0.29	209.44	0.678	0.671	0.671
2-PU	0.58	242.10	0.783	0.776	0.776
4-PU	1.16	267.74	0.866	0.858	0.858
6-PU	1.74	279.36	0.904	0.895	0.895
Titanium (Ti)	22	309.03	1	0.990	0.990
Aluminum (Al)	236	312.05	1.010	1	1.000
Copper (Cu)	398	312.18	1.010	1.000	1

compared with the experimental ones, as illustrated in Fig. 7 and Fig. 8. It worth noting that the aim of theoretical models is to provide upper and lower limits of the experimental performance, instead of validating experimental results.

Fig. 7 shows the global heat transfer rate obtained from the experimental, parallel flow and crossflow theoretical models. It shows that the experimental result is in between the data provided by

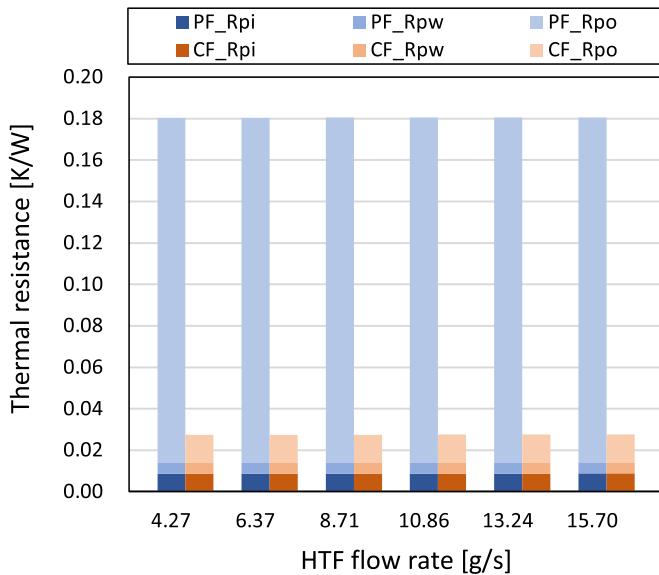


Fig. 9. Thermal resistances of peripheric pipes in the cases of parallel flow and crossflow.

parallel flow and crossflow correlations. Comparing with the experimental results, the crossflow theoretical model gives 34%–64% higher global heat transfer rate in the studied range of HTF flow rate, of which 64% occurs at the highest HTF flow rate of 15.70 g/s; while the values are 50%–62% lower in the parallel flow. Therefore, it can be concluded that the actual flow in the heat exchanger during experimental runs is neither pure parallel flow nor crossflow, but a combination of the two.

Fig. 8 shows similar trends in terms of the global heat transfer coefficient. Compared with the experimental results, which range from 100 to 110 W/m<sup>2</sup>·K, the theoretical overall heat transfer coefficient in crossflow could double the experimental performance, whereas the coefficient in parallel flow could be reduced to 1/3. In other words, the theoretical model in crossflow and parallel flow prescribe an upper and a lower limit of thermal performance to the actual flow in the heat exchanger. Moreover, as the HTF flow rates increase and the corresponding internal flow regime turns from laminar to turbulent flow, the global heat transfer coefficient keeps stable for all three data series. This implies that the global heat transfer coefficient might be mainly limited by the external convection or the heat conduction through walls, instead of the internal convection.

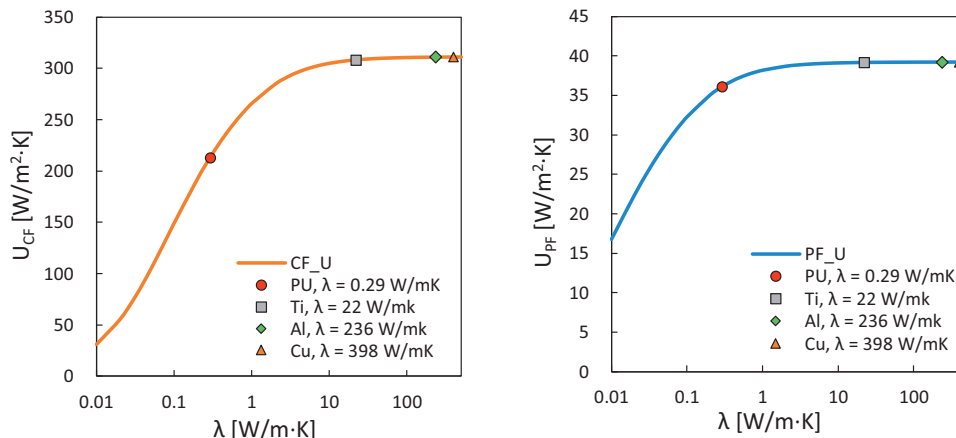


Fig. 10. Theoretical relation between global heat transfer coefficient and material thermal conductivity in the case of crossflow (left) and parallel flow (right) (working conditions:  $\dot{m}_{HTF} = 10.86$  g/s,  $T_{HTF,in} = 20.7^\circ\text{C}$ ,  $T_{w,in} = 30.1^\circ\text{C}$ ,  $\dot{m}_w = 60$  g/s).

Table 3

Performance comparison between heat exchanger made of different materials in parallel flow.

Heat exchanger material	$\lambda$ [W/m·K]	$U$ [W/m <sup>2</sup> ·K]	$U/U_{Ti}$	$U/U_{Al}$	$U/U_{Cu}$
Polyurethane (PU)	0.29	36.18	0.920	0.919	0.919
2-PU	0.58	37.62	0.957	0.956	0.956
4-PU	1.16	38.45	0.978	0.977	0.977
6-PU	1.74	38.75	0.985	0.984	0.984
Titanium (Ti)	22	39.32	1	0.999	0.999
Aluminum (Al)	236	39.37	1.001	1	1.000
Copper (Cu)	398	39.37	1.001	1.000	1

#### 5.4. Thermal resistances

As over 87% of the global heat transfer rate is exchanged through the peripheric pipes, only the thermal resistances of the peripheric part is studied in this section. Fig. 9 illustrates the influence of HTF flow rates and flow patterns (parallel flow and crossflow) on the three thermal resistances of peripheric pipes ( $R_{pi}$ ,  $R_{pw}$ , and  $R_{po}$ ). Clearly, the total thermal resistance is considerably lower in crossflow than parallel flow, by a factor of about 7. Since the internal Dean flow for the case of crossflow pattern is considered negligible in this study, the only difference between parallel and crossflow lies in the external convection. It shows that external convective thermal resistance is the principal resistance in both flow patterns, accounting for more than 90% of the total thermal resistance in parallel flow and about 50% in crossflow. This is due to the influence of a considerably lower external convective heat transfer coefficient caused by a larger hydraulic diameter on the external surface in comparison with the internal one. Therefore, the increase of HTF flow rates, which enhances the internal convection only, has little influence on the global thermal resistances in all flow rates and for both flow patterns. More importantly, comparing the three thermal resistances, the wall resistance in peripheric pipes ( $R_{pw}$ ) is the lowest. The use of low-conductivity polymer can be potentially competitive to metal-made heat exchangers. Since the situation is slightly different in the central pipe, global heat exchange coefficient should be used to investigate the influence of thermal conductivity.

#### 5.5. Comparison with metal heat exchangers

With the theoretical model, the material thermal conductivity is studied to determine its effects on the thermal performance of the heat exchanger in both cases of parallel flow and crossflow. The results obtained with PU ( $\lambda = 0.29$  W/m·K) are



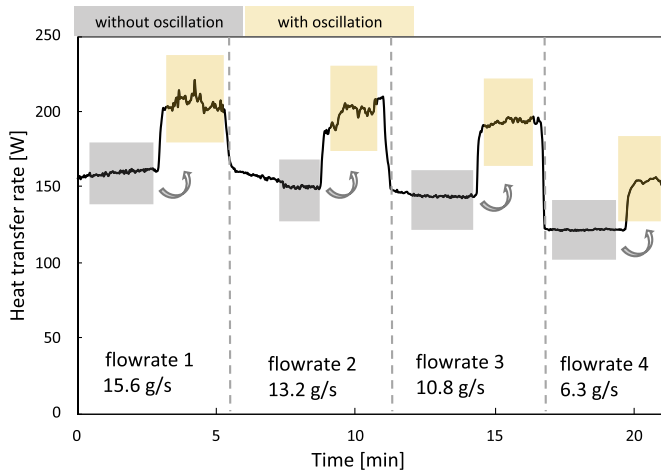


**Fig. 11.** Heat transfer rates comparison between fixed and oscillation positions at different HTF flow rates.

compared with three selected metal heat exchangers, titanium, aluminum, and copper, whose thermal conductivity are 22 W/m·K, 236 W/m·K, and 398 W/m·K, respectively. The global heat transfer coefficient is used as bases for comparison under the same working conditions:  $\dot{m}_{HTF} = 10.86 \text{ g/s}$ ,  $T_{HTF,in} = 20.7^\circ\text{C}$ ,  $T_{w,in} = 30.1^\circ\text{C}$ ,  $\dot{m}_w = 60 \text{ g/s}$ . Three fictive PU with their thermal conductivities multiplied by a factor of 2, 4, and 6 are also analysed.

Fig. 10 shows the theoretical results of the global heat transfer coefficient as a function of thermal conductivity in the case of crossflow and parallel flow. The detailed comparison results, as well as their relative performance ratios to each metal heat exchanger, are listed in Tables 2 and 3. The polymer heat exchanger shows promising performance compared with conventional metal ones with the same dimension and working conditions. For crossflow in Fig. 10, the polymer heat exchanger is expected to have a U-value of 209.44 W/m<sup>2</sup>·K, while the best metal performance (Copper) gives 312.18 W/m<sup>2</sup>·K. For parallel flow, the values are respectively 36.18 W/m<sup>2</sup>·K and 39.37 W/m<sup>2</sup>·K. From the comparison results in Tables 2 and 3, it is clear that the thermal performance of the heat exchanger made of PU can achieve about 67% and 92% of the titanium, aluminum, or copper heat exchanger in crossflow and parallel flow, respectively. If the thermal conductivity is doped

by a factor of 6, reaching 1.74 W/m·K, the heat exchanger performance can achieve about 90% and 99% of the three selected metal materials, respectively in crossflow and parallel flow. As previously discussed, the experimental performance of PU-made heat exchanger is limited by the parallel flow and crossflow models, it is reasonable to conclude that the heat exchanger can achieve a performance of 67%-92% of titanium, aluminum, or copper heat exchangers.

Fig. 10 also provides a design guide for polymer heat exchangers in terms of material choice. In the case of crossflow, there is a critical value (about 5.0 W/m·K) of material thermal conductivity that divides the performance curve into two parts. Below this value, the curve is very sharp, which means that improving thermal conductivity will considerably boost the heat exchanger thermal performance. However, over this value, the curve tends to be flat at 312 W/m·K and thus improving thermal conductivity contributes very little to the heat performance enhancement. In the case of parallel flow, the important critical value is about 1 W/m·K. Above this value, increasing thermal conductivity has little effect on the curve since U-value tends to stay at a constant global heat transfer coefficient of approximately 40 W/m<sup>2</sup>·K. From the heat exchange performance point of view, improving thermal conductivity is worthless after the critical value since the main thermal resistance comes from the convective heat transfer, in particular the external one, rather than the pipe heat conduction (see Fig. 9). As the real serpentine shape heat exchanger should be in between parallel and crossflow, the critical heat conductivity should be between 1 and 5 W/m·K.

5.6. Performance enhancement by oscillation – preliminary results

As one of the advantages of using soft material, oscillation and its influence on thermal performance is studied experimentally. Manually agitation of the heat exchanger around its longitudinal axis creates serpentine-like movement with transient deformation. As described earlier, the heat exchanger deforms as an external force is applied, either from mechanical shaking or from the natural flow of the source side fluid. Fig. 11 shows some preliminary experimental results of the heat transfer rate for a continuous experimental run at four different HTF flow rates. It is found that oscillation significantly improves thermal performance by more than 30% regardless of the HTF flow rates. This is presumably due to the disturbance of the flow characteristics by movement,

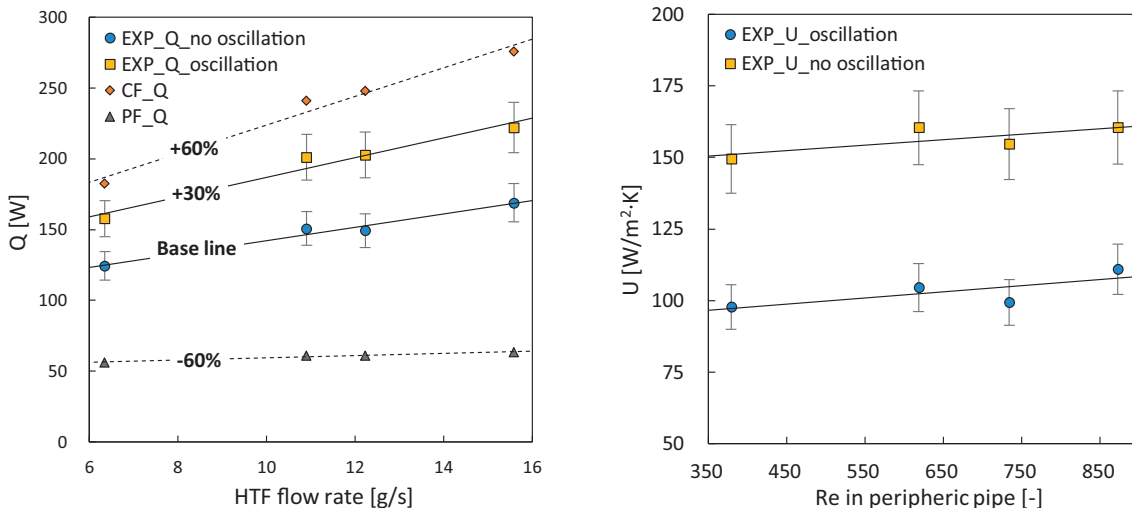


**Fig. 12.** Heat transfer improvement by oscillation of the heat exchanger in the source-side fluid: (left) experimental results and theoretical limits and (right) experimental global heat transfer coefficients with respect to Re.

which perturbs the thermal boundary layer and thus improves the external heat convection. As previously discussed, results from the theoretical model indicate that principal thermal resistance lies in the external convection between the pipe and source-side fluid. Disturbance from manual shaking allows a continuous reduction of the thermal boundary layer since the flow pattern alternates between parallel flow and crossflow. As a result, the crossflow pattern would be more pronounced than in a stationary situation.

The thermal performance improvement by movement can be better illustrated by comparing the experimental results (with and without oscillation) with the theoretical performance limits (parallel flow and crossflow) under the same working conditions, as shown in Fig. 12 (left). Compared with the stationary case, a clear increase of 30% in heat transfer rate is observed for the heat exchanger under oscillation, which suggests an enhanced thermal performance closer to that of crossflow (+60%). However, the performance is still within the theoretical performance range limited by parallel flow and crossflow correlations. It offers evidence that more crossflow pattern is presenting in the heat exchanger subjected to oscillational movement. The major heat transfer enhancement under oscillation may be explained by plotting the global heat transfer coefficient against  $Re$  in peripheral pipes, as shown in Fig. 12 (right). In peripheral pipes,  $Re$  ranges from 379 to 873 with corresponding HTF flow rates from 6.35 to 15.59 g/s. A significant rise in the global heat transfer coefficient by about 50% can be observed for the heat exchanger under movement.

## 6. Conclusions and perspectives

In this paper, a patented soft polymer heat exchanger for wastewater heat recovery is studied to explore its heat transfer characteristics, including heat transfer rate, heat transfer coefficient, and thermal resistance. The effect of material thermal conductivity and oscillation on the thermal performance justifies the interests of the novel heat exchanger. Both experiments and theoretical calculations are carried out.

Experimental results show a global heat transfer coefficient between 100–110  $W/m^2 \cdot K$  for an HTF flow rate of 4.27–15.70 g/s and 60 g/s at the source side. It is further found that with a heat transfer area three times larger than the central pipe, the peripheral pipes are largely dominating (over 87%) the performance of the heat exchanger in terms of heat transfer rate. In addition, when subjected to a manually assisted serpentine-like movement, the heat exchanger shows a significantly better performance, with an increase of about 30% compared with a stationary situation.

The theoretical models demonstrate that the performance of the polymer heat exchanger is in between the parallel and crossflow heat exchangers with the same configuration. More specifically, the experimental global heat transfer rate is up to 64% lower than the theoretical value in crossflow while up to 62% higher than those estimated by the parallel flow model. Hence, it reveals that the actual flow pattern in the experiment is a combination of parallel flow and crossflow. In terms of thermal resistance, theoretical results confirm that the external convective thermal resistance is the dominant one, and the low thermal conductivity of polymer does not significantly deteriorate the global heat transfer coefficient.

With the theoretical models, a sensitivity study on the material thermal conductivity on heat exchanger performance is investigated. The results show that there is a critical value that divides the performance curve of the heat exchanger into two parts. Below this value, improving thermal conductivity will considerably boost the heat exchanger performance while over this value improving thermal conductivity contributes very little to the heat

performance enhancement. This critical value is about 5.0  $W/m \cdot K$  in the crossflow heat exchanger and 1.0  $W/m \cdot K$  in the parallel flow heat exchanger. For the specific polymer heat exchanger made of polyurethane in this paper, it can reach 67% and 92% of the titanium, aluminum, and copper heat exchanger performance in crossflow and parallel flow, respectively. It can be concluded that using polymer materials to make heat exchangers can be thermally competitive to the conventional metal-based heat exchangers.

The polymer heat exchanger presented in this paper shows high potentiality to be used in the wastewater heat recovery application, not only because of the merits of using polymer materials but also its unique adaption to the installation environment. Firstly, it is flexible and can be changed to any shape as required. Secondly, due to the low weight, it always floats on the upper part of the wastewater where the water temperature is usually higher than the bottom part. In this way, the heat transfer between wastewater and HTF can be maximized. As mentioned previously, the heat exchanger performance potentially can be further improved in a crossflow environment or under movement. Future works will be focused on the study of heat transfer enhancement by vibration with different frequencies and amplitudes preferably induced by source-side fluid. Other perspectives include the implementation of the polymer heat exchanger in a real case with specific environments.

## Declaration of Competing Interest

The authors declare that they have no known competing financial interests or personal relationships that could have appeared to influence the work reported in this paper.

## Acknowledgements

The authors would like to acknowledge research supports provided by Erganeo (France), I-SITE FUTURE (France), ERASMUS program (European Union) as well as China Scholarship Council (P.R. China).

## Appendices

### A1. Pressure loss

The pressure drop through the HTF side is measured by an AST5100 wet-wet differential pressure transmitter. HTF flowrate ranges from 4.3 to 15.7 g/s, and it the same with the thermal performance part. The pressure loss follows a logarithmic trend with respect to the mass flowrate, and its maximal and minimum values are respectively 7 132 Pa and 24 588 Pa for the total length of 1.65 m (Fig. A1).

### A2. Validation of LMTD with $NUT-\epsilon$ method

In order to validate theoretical results calculated from the LMTD method,  $NTU-\epsilon$  method is used. The heat transfer rate is calculated separately for the peripheral pipe and central pipe. As the calculation procedures are the same, here taking the peripheral pipe as an example. The heat capacity rates ( $C$ ) for the two fluids are determined as shown in Eqs. (32)–(33). The heat capacity ratio ( $C_r$ ) is then the minimum value to the maximum value of the two heat capacity rates ( $C_{HTF}, C_w$ ).

$$C_{HTF} = \dot{m}_{HTF} c_{p,HTF} \quad (32)$$

$$C_w = \dot{m}_w c_{p,w} \quad (33)$$

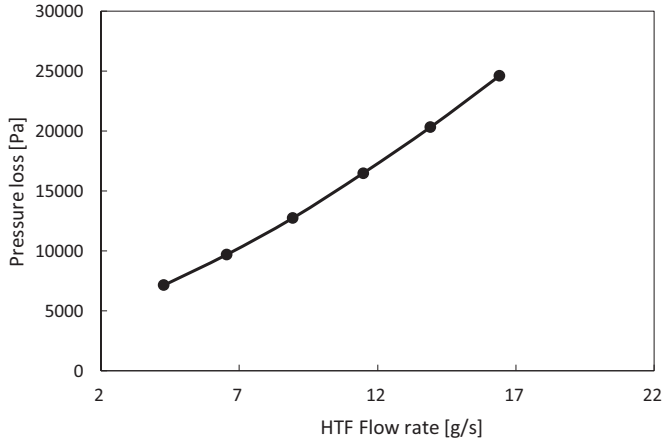


Fig. A1. HTF side pressure loss at the full range of flow rates.

$$C_r = \frac{\min(C_{HTF}, C_w)}{\max(C_{HTF}, C_w)} \quad (34)$$

The Number of Transfer Units (NTU) is defined as:

$$NTU = \frac{(UA)_p}{\min(C_{HTF}, C_w)} \quad (35)$$

The effectiveness ( $\varepsilon$ ) is then estimated from Eqs. (36)-(37) depending on the flow patterns in the pipe [27]:

$$\varepsilon_p = \frac{1 - \exp[-NTU(1 + C_r)]}{1 + C_r} \quad (\text{in parallel flow, peripheric pipe}) \quad (36)$$

$$\varepsilon_c = \frac{1 - \exp[-NTU(1 - C_r)]}{1 - C_r \exp[-NTU(1 - C_r)]} \quad (\text{in crossflow, } C_r < 1, \text{ central pipe}) \quad (37)$$

Finally, the heat transfer rate can be evaluated according to Eqs. (38)-(39) from the above calculated results. The global heat transfer rate is calculated using Eq. (27).

$$\dot{Q}_p = \varepsilon_p \cdot \min(C_{HTF}, C_w)(T_{w,in} - T_{HTF,in}) \quad (38)$$

$$\dot{Q}_c = \varepsilon_c \cdot \min(C_{HTF}, C_w)(T_{w,in} - T_{HTF,m}) \quad (39)$$

With the heat transfer rates, the outlet temperatures can be determined as follows:

$$T_{HTF,m} = T_{HTF,in} + \frac{\dot{Q}_p}{C_{HTF}} \quad (40)$$

$$T_{HTF,out} = T_{HTF,m} + \frac{\dot{Q}_c}{C_{HTF}} \quad (41)$$

$$T_{w,out} = T_{w,in} - \frac{\dot{Q}}{C_w} \quad (42)$$

The comparison results of the HTF outlet temperature in crossflow derived from LMTD and NTU- $\varepsilon$  methods are illustrated in Fig. A2. The results obtained from LMTD method are numerically in line with that from NTU- $\varepsilon$  method. The temperature differences between two methods are only 0.1°C and 0.05°C respectively at the HTF middle and outlet locations, which indicates that the LMTD method is highly accurate.

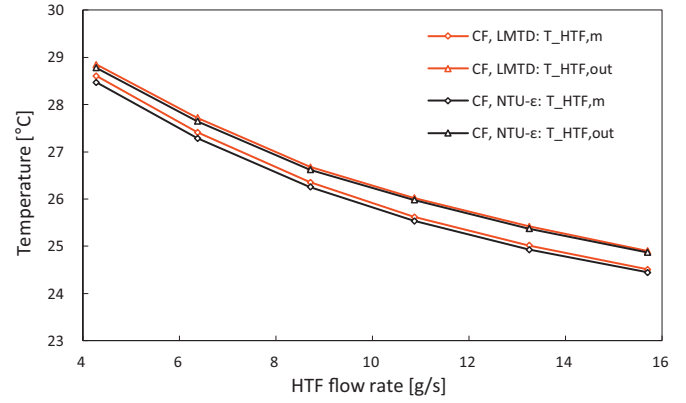


Fig. A2. A comparison between the HTF outlet temperatures in crossflow as calculated from LMTD and NTU- $\varepsilon$  methods.

## References

- [1] Energy Information Administration (EIA), International Energy Outlook 2019, (2019). <https://www.eia.gov/outlooks/ieo/pdf/ieo2019.pdf> (accessed April 8, 2020).
- [2] International Energy Agency (IEA), Cities are at the frontline of the energy transition, (2016). <https://www.iea.org/news/cities-are-at-the-frontline-of-the-energy-transition> (accessed April 8, 2020).
- [3] X. Guo, A.P. Goumba, C. Wang, Comparison of direct and indirect active thermal energy storage strategies for large-scale solar heating systems, *Energies* (2019) 12, doi:10.3390/en12101948.
- [4] X. Hao, J. Li, M.C.M. Van Loosdrecht, H. Jiang, R. Liu, Energy recovery from wastewater, *Heat Over Organics* (2019), doi:10.1016/j.watres.2019.05.106.
- [5] A. Mazhar, S. Liu, A. Shukla, A key review of non-industrial greywater heat harnessing, *Energies* 11 (2018) 386, doi:10.3390/en11020386.
- [6] I. Takashi, A. Toshiya, H. Keisuke, Life cycle inventory analyses for CO2 emission and cost of district heating and cooling systems using wastewater heat (in Japanese), *J. JSCE (Japan Soc. Civ. Eng. Div. D Environ. Syst. Eng.* 64 (2008) 107–122.
- [7] X. Guo, M. Hendel, Urban water networks as an alternative source for district heating and emergency heat-wave cooling, *Energy* 145 (2018) 79–87, doi:10.1016/j.energy.2017.12.108.
- [8] J.P. van der Hoek, S. Mol, S. Giorgi, J.I. Ahmad, G. Liu, G. Medema, Energy recovery from the water cycle: Thermal energy from drinking water, *Energy* 162 (2018) 977–987, doi:10.1016/j.energy.2018.08.097.
- [9] CELSIUS, Waste heat recovery from sewage water in Cologne, Germany, (2020). <https://celsiustcity.eu/waste-heat-recovery-from-sewage-water-in-cologne-germany/> (accessed May 4, 2020).
- [10] CELSIUS, Excess heat from sewage in Hamburg and Singen, Germany, (2020). <https://celsiustcity.eu/excess-heat-from-sewage-in-hamburg-and-singen-germany/> (accessed May 4, 2020).
- [11] A. Goumba, S. Chiche, X. Guo, M. Colombert, P. Bonneau, Recov'Heat: An estimation tool of urban waste heat recovery potential in sustainable cities. in, *AIP Conference Proceedings* 1814 (2017), doi:10.1063/1.4976257.
- [12] Veolia, Opening of a new Energido unit in Aix-les-Bains: Veolia transforms into wastewater to produce energy, (2015). <https://www.veolia.com/en/veolia-group/media/news/opening-new-energido-unit-aix-les-bains-veolia-recycles-wastewater-produce-energy> (accessed May 4, 2020).
- [13] D.J. Dürrenmatt, O. Wanner, A mathematical model to predict the effect of heat recovery on the wastewater temperature in sewers, *Water Res.* 48 (2014) 548–558, doi:10.1016/j.watres.2013.10.017.
- [14] L. Chen, Z. Li, Z.Y. Guo, Experimental investigation of plastic finned-tube heat exchangers, with emphasis on material thermal conductivity, *Exp. Therm. Fluid Sci.* 33 (2009) 922–928, doi:10.1016/j.expthermflusci.2009.04.001.
- [15] H. Bart, S. Scholl (Eds.), *Innovative Heat Exchangers*, Springer International Publishing, AG, Cham, Switzerland, 2018, doi:10.1007/978-3-319-71641-1.
- [16] A. Laval, Alfa Laval brochure-spiral heat exchangers, n.d. <http://www.heat-transfer-solutions.com/documents/alfa-laval-spiral-heat-exchanger-brochure.pdf> (accessed May 4, 2020).
- [17] X. Chen, Y. Su, D. Reay, S. Riffat, Recent research developments in polymer heat exchangers - A review, *Renew. Sustain. Energy Rev.* 60 (2016) 1367–1386, doi:10.1016/j.rser.2016.03.024.
- [18] O. Breuer, U. Sundararaj, Big returns from small fibers: a review of polymer/carbon nanotube composites, *Polym. Compos.* 25 (2004) 630–645.
- [19] Y.P. Mamunya, V.V. Davydenko, P. Pissis, E.V. Lebedev, Electrical and thermal conductivity of polymere filled with metal powders, *Eur. Polym. J.* 38 (2002) 1887–1897.
- [20] J. Shi, J. Hu, S.R. Schafer, C.L. Chen, Numerical study of heat transfer enhancement of channel via vortex-induced vibration, *Appl. Therm. Eng.* 70 (2014) 838–845, doi:10.1016/j.applthermaleng.2014.05.096.

- [21] W. Liu, Z. Yang, B. Zhang, P. Lv, Experimental study on the effects of mechanical vibration on the heat transfer characteristics of tubular laminar flow, *Int. J. Heat Mass Transf.* (2017), doi:[10.1016/j.ijheatmasstransfer.2017.07.025](https://doi.org/10.1016/j.ijheatmasstransfer.2017.07.025).
- [22] S.W. Chen, F.C. Liu, H.J. Lin, P.S. Ruan, Y.T. Su, Y.C. Weng, J.R. Wang, J. Der Lee, W.K. Lin, Experimental test and empirical correlation development for heat transfer enhancement under ultrasonic vibration, *Appl. Therm. Eng.* 143 (2018) 639–649, doi:[10.1016/j.applthermaleng.2018.07.133](https://doi.org/10.1016/j.applthermaleng.2018.07.133).
- [23] M. Legay, B. Simony, P. Boldo, N. Gondrexon, S. Le Person, A. Bontemps, Improvement of heat transfer by means of ultrasound: Application to a double-tube heat exchanger, *Ultrason. Sonochem.* 19 (2012) 1194–1200, doi:[10.1016/j.ultrasonch.2012.04.001](https://doi.org/10.1016/j.ultrasonch.2012.04.001).
- [24] M. Legay, O. Bulliard-Sauret, S. Ferrouillat, P. Boldo, N. Gondrexon, Methods to evaluate heat transfer enhancement in an ultrasonic heat exchanger, *Heat Transf. Eng.* (2019) 1–16, doi:[10.1080/01457632.2019.1649917](https://doi.org/10.1080/01457632.2019.1649917).
- [25] X. Guo, Flexible heat exchanger intended to be positioned in a moving exterior fluid, comprising a collection of flexible temperature probes, WO2020049233A1, 2020.
- [26] H. Wang, L. Balasubramaniam, S.D. Marshall, X. Jin, R. Arayanarakool, P.S. Lee, P.C.Y. Chen, Numerical study of heat transfer enhancement of roll-to-roll microchannel heat exchangers, *J. Heat Transfer* 140 (2018) 1–8, doi:[10.1115/1.4038910](https://doi.org/10.1115/1.4038910).
- [27] T.L. Bergman, A.S. Lavine, F.P. Incropera, D.P. Dewitt, *Fundamental of Heat and Mass Transfer, Seventh Ed*, John Wiley & Sons, 2011.
- [28] S.W. Churchill, Friction-factor equation spans all fluid-Flow regimes, *Chem. Eng. (New York)*. 84 (1977) 91–92.
- [29] W.M. Rohsenow, J.P. Hartnett, Y.I. Cho, *Handbook of heat transfer*, Third Edit, McGraw-Hill, New York, 1998, doi:[10.5860/choice.36-3347](https://doi.org/10.5860/choice.36-3347).
- [30] R. Karwa, *Heat and Mass Transfer*, Springer, Singapore, 2017, doi:[10.1007/978-981-10-1557-1](https://doi.org/10.1007/978-981-10-1557-1).